Journal of Materials Chemistry C

ROYAL SOCIETY OF CHEMISTRY

PAPER

View Article Online
View Journal | View Issue

Cite this: J. Mater. Chem. C, 2026, 14, 4451

Selective fluorescence detection of cholesterol using an anthracene–triazole probe: a turn-on, enzyme/metal-free approach

Rakhi Mol K M[a] and Mintu Porel *[ab]

Received 29th October 2025,
Accepted 15th December 2025

DOI: 10.1039/d5tc03858h

rsc.li/materials-c

Cholesterol is a fundamental lipid found in animal cells, serving as a precursor in the biosynthesis of several hormones and essential vitamins. Accurate detection of cholesterol is critical for the early diagnosis and effective monitoring of cholesterol-related disorders, including cardiovascular diseases and liver diseases. Herein, we report a rapid and straightforward enzyme- and metal-free strategy for cholesterol detection using an anthracene–triazole fluorescent molecule, **ATBz**, synthesized *via* copper-catalyzed azide–alkyne click reaction (CuAAC). The synthesized **ATBz** was thoroughly characterized using various techniques, including ^{1}H and ^{13}C NMR, LC-MS, FT-IR, and UV-vis absorption and emission spectroscopy. Interestingly, the **ATBz** molecule exhibits selective interaction with cholesterol, resulting in a fluorescence turn-on response characterized by bright green emission and a slight blue shift of about 12 nm ($\Delta\lambda$). The presence of cholesterol is proposed to facilitate the formation of rigid assemblies, which restrict the molecular motion of **ATBz** and trigger aggregation-induced emission. It exhibits a limit of detection (LOD) of (100 ± 1.4) nM and a binding constant of (1.29 ± 0.24) × 10^5 M^{-1}. The observed fluorescence enhancement was further validated through time-correlated single photon counting (TCSPC), quantum yield measurements, FESEM, PXRD and NMR analyses. The practical applicability of **ATBz** was evaluated in real samples, including egg yolk, human serum, and goat blood. Furthermore, a paper-based test strip was developed for cholesterol detection, highlighting its potential utility in clinical diagnostics.

Introduction

Cholesterol is a vital component of mammalian tissues and cells, playing a key role in various biological functions.[1,2] These include the synthesis of steroid hormones, bile acids, and vitamin D, as well as contributing to membrane stability and fluidity.[3] The normal range of cholesterol in human serum typically lies between 3.23 mM (125 mg dL^{-1}) and 5.17 mM (200 mg dL^{-1}).[4] Deviations from this range can lead to significant health concerns. Elevated cholesterol levels are associated with the development of atherosclerotic plaques, increased blood pressure, stroke, cardiovascular diseases, hypertension, type 2 diabetes, and venous thrombosis.[5,6] Conversely, abnormally low cholesterol levels can result in anaemia, weakened immune response, depression, Tangier disease, and haemorrhagic stroke.[7–10] Therefore, regular monitoring of serum cholesterol is crucial for preventive healthcare and plays a significant role in reducing the risk of heart-related and associated conditions.

Currently, a variety of methods are employed to detect cholesterol in human serum, including colorimetry,[11] chromatography-mass spectrometry,[12] enzymatic assays,[13] electrochemical techniques,[14] molecular imprinting technologies,[15] and fluorescence-based approaches.[16] Among these, for clinical purpose, enzyme-dependent methods are commonly used for cholesterol quantification. However, these methods often face challenges such as limited stability, high costs associated with enzyme extraction and purification, and susceptibility to environmental factors, which restrict their broader applications.[17] In contrast, fluorescence-based detection techniques have attracted considerable attention due to their high sensitivity and selectivity, rapid response, simple mode of operation, and minimal sample requirement.[18] In recent years, a variety of fluorescent nanomaterial-based sensors have been engineered for the detection of cholesterol. These sensors span from simple nanostructures, such as individual nanoparticles and quantum dots, to more complex hybrid nanocomposite systems.[19] For example, Ye *et al.*[20] introduced a highly sensitive fluorescence assay that utilizes green-emitting silicon nanoparticles (SiNPs) as the sensing element and *p*-phenylenediamine oxide (PPDox) as a quencher. Similarly, Sultana *et al.*[21] developed a non-enzymatic cholesterol sensor based on phosphorene quantum dots functionalized with silk fiber (Ph–SF), where fluorescence is restored *via*

[a] Department of Chemistry, Indian Institute of Technology Palakkad, Kerala, 678557, India. E-mail: mintu@iitpkd.ac.in
[b] Environmental Sciences and Sustainable Engineering Center, Indian Institute of Technology Palakkad, Kerala, 678557, India

the inner filter effect (IFE) upon interaction with cholesterol. In another advancement, Dolai *et al.*[22] constructed a molecularly imprinted nanocomposite comprising polycyclodextrin and graphene oxide, which enables selective and enzyme-free detection of cholesterol through a fluorescence "turn-on" mechanism driven by indicator displacement. In contrast to nanomaterial-based sensors, organic fluorescent molecules offer significant advantages owing to their well-defined and stable molecular structures, which enhance sensor robustness and enable precise recognition mechanisms. For instance, Kaur *et al.*[23] reported an enzyme- and metal-free quinoxaline-based probe (QxPyA) that achieved direct light-up detection of cholesterol in aqueous media and human serum. In this system, cholesterol binding induces hydrophobicity and structural rigidity within the probe's supramolecular assemblies, resulting in a pronounced and highly selective fluorescence enhancement. Wu *et al.*[24] developed a cyanostilbene-based double-ionic macrocyclic fluorescence sensor in which cholesterol binds within the macrocyclic cavity through hydrogen bonds and hydrophobic interactions, restricting aromatic rotation and decreasing solubility, thereby enhancing aggregation-induced emission and shifting fluorescence from green-yellow to green-blue.

Numerous cholesterol detection strategies based on enzymatic systems, MOFs, and nanoparticle platforms have been reported (Table S1); however, these methods typically exhibit micromolar LODs and often require relatively long detection times. In contrast, small-molecule fluorescent probes remain comparatively underexplored, with only a limited number of examples employing small organic molecules or macrocyclic systems for cholesterol sensing. Herein, we report a simple anthracene–triazole-based small molecular system (**ATBz**), efficiently synthesized *via* copper-catalyzed azide–alkyne click reaction (CuAAC). Although the reported probes achieve lower LODs than **ATBz**, we consider **ATBz** to be a meaningful addition to this emerging class of sensors. **ATBz** offers synthetic simplicity, high yield, good stability, a metal-free design, and a rapid fluorescence turn-on response, making it a straightforward and practical alternative to more complex existing methods. The anthracene fluorophore contributes significantly to the photophysical behaviour owing to its extended aromatic framework and conjugated π-system. Since cholesterol is known to induce subtle changes in hydrophobicity, polarity, and viscosity within the local microenvironment, the **ATBz** system exhibits fluorescence enhancement and a characteristic green emission upon interaction, driven by aggregation-induced emission (AIE). Furthermore, cholesterol detection was successfully demonstrated in human serum, goat blood, and egg yolk samples and on paper strips. Overall, this represents a straightforward, enzyme- and metal-free fluorescent platform for the selective and sensitive quantification of cholesterol in aqueous and biological media.

Experimental section

Materials and methods

All the chemicals were obtained from Sigma-Aldrich, Alfa Aesar, Spectrochem, Nice, Merck, and TCI and were used as received without any further purification.

Instrumentation

All LC-MS analyses were performed using a Shimadzu LC-MS-8045 equipped with a Sprite TARGA C18 column (40 × 2.1 mm, 5 μm). Detection was carried out at 210 and 254 nm in positive ionization mode. The mobile phases consisted of water containing 0.1% formic acid (solvent A) and acetonitrile with 0.1% formic acid (solvent B). The gradient program was as follows: 5% solvent B for 2 min, a linear increase from 5% to 40% over 4 min, followed by a gradual rise from 40% to 60% over 10 min. The system was then returned to 5% solvent B within 2 min and maintained for an additional 2 min before termination. Prior to each injection, the column was conditioned sequentially with 50% and 95% solvent B. ^{1}H and ^{13}CNMR spectra were acquired on a Bruker AV III 400 MHz instrument and processed using MestReNova (v. 8.1.1). Chemical shifts are reported in ppm relative to tetramethylsilane (TMS) as the internal standard, and data are presented as chemical shift, multiplicity (s = singlet, d = doublet, t = triplet, and m = multiplet), and proton count. Fluorescence measurements were recorded on a PerkinElmer FL 6500 spectrofluorometer, while absorption and emission spectra were plotted using OriginPro 8.5.1. All fluorescence emission spectra were collected at 25 °C using an excitation wavelength of 296 nm. Lifetime measurements were carried out using a time-correlated single-photon counting (TCSPC) system (HORIBA Deltaflex) equipped with a 340 nm nano-LED excitation source with an instrument response function of 1 ns.

Design and synthetic strategies of ATBz

The synthesis of **ATBz** was accomplished through a straightforward and concise three-step route, as outlined in Scheme 1. The synthetic strategy begins with the reaction of 2-aminoanthracene **1** with propargyl bromide in dimethylformamide (DMF) at 0 °C, yielding compound **2**. Benzyl bromide, **3**, was then converted to the corresponding azide using sodium azide, affording compound **4**. Finally, the target molecule **ATBz** was synthesized *via* a copper(I)-catalyzed azide–alkyne cycloaddition (CuAAC) "click" reaction between dialkyne **2** and diazide **4**, resulting in a 70% yield (Scheme 1). MS (ESI) *m*/*z*: $[M + H]^+$ calculated for $C_{34}H_{29}N_7$

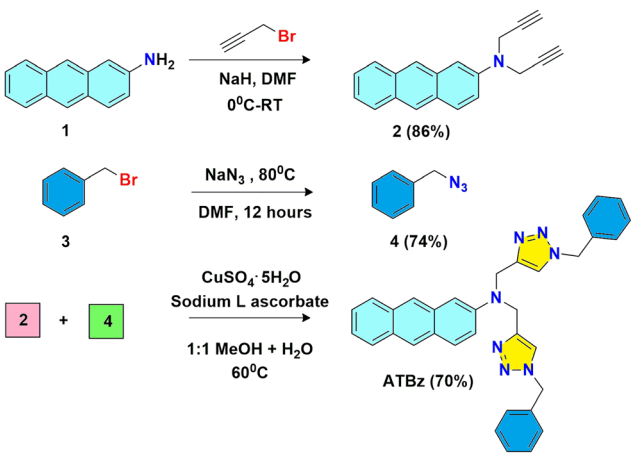

Scheme 1 Synthesis of **ATBz**.

536.25; found 536.50. ^{1}H NMR (400 MHz, $CDCl_3$) δ 8.24 (s, 1H), 8.08 (s, 1H), 7.92–7.83 (m, 3H), 7.42–7.33 (m, 3H), 7.32 (s, 2H), 7.29–7.26 (m, 6H), 7.15 (dd, J = 3.9, 2.0 Hz, 4H), 7.08 (d, J = 2.3 Hz, 1H), 5.41 (s, 4H), 4.74 (s, 4H). ^{13}C NMR (101 MHz, $CDCl_3$) δ 145.50 (s), 145.04 (s), 134.62 (s), 132.90 (s), 132.40 (s), 129.98 (s), 129.54 (s), 129.06 (s), 128.65 (s), 128.21 (s), 127.82 (s), 127.60 (s), 127.20 (s), 125.93 (s), 124.00 (s), 123.35 (s), 122.16 (s), 118.94 (s), 106.81 (s), 54.32–54.13 (m), 46.93 (s).

General procedure for fluorescence studies

A 2 mM stock solution of **ATBz** was prepared in DMSO and subsequently diluted with distilled water to obtain the desired concentrations for fluorescence measurements. Additionally, a 10 mM stock solution of cholesterol was prepared in ethanol. Stock solutions (50 mM) of various analytes – arginine, cysteine, glutamic acid, histidine, phenylalanine, serine, tryptophan, valine, ascorbic acid, $CaSO_4$, creatinine, dopamine, glucose, KCl, $MgSO_4$, NaCl, sucrose, urea, and uric acid – were prepared in water. The fluorescence spectra were recorded using a 10 μM solution in a quartz cuvette at 25 °C, with an excitation wavelength of 296 nm and a scan speed of 240 nm s^{-1}. The detailed experimental procedures are provided in the SI.

Lifetime measurement

A 2 mM stock solution of **ATBz** was prepared in DMSO. For TCSPC analysis, 10 μM of this stock solution was diluted in 2 mL of water containing 0.5% DMSO. Subsequently, cholesterol was added to the solution at concentrations of 10 μM and 50 μM, and the fluorescence decay profiles were recorded for each case.

Recovery of cholesterol in human serum

A 2 mM stock solution of **ATBz** was prepared in DMSO, and a calibration curve of I/I_0 *versus* cholesterol concentration was constructed from fluorescence spectra, where I_0 denotes the fluorescence intensity of **ATBz** alone and I denotes the intensity after cholesterol addition. For serum analysis, 10 μL of artificial human serum was first diluted tenfold with buffer. From this diluted stock, 200 μL was further mixed with 1790 μL of buffer and 10 μL of **ATBz** solution. To evaluate cholesterol recovery, known amounts of cholesterol were spiked into the serum samples at concentrations of 1 μM, 100 μM, 0.5 mM, and 1 mM. The fluorescence spectra of these spiked samples were then recorded. Finally, the cholesterol concentrations were quantified using the previously established calibration curve.

Detection of cholesterol in egg yolk

1 g of egg yolk was dispersed in 20 mL of water, stirred, and then treated ultrasonically for 20 minutes. The resulting mixture was left to settle and subsequently filtered to obtain a clear extract, which was further diluted with water to a total volume of 100 mL. For fluorescence analysis, 2 mL of a 10 μM aqueous **ATBz** solution was placed in a cuvette, and its spectrum was recorded. In a parallel experiment, an identical concentration of **ATBz** (10 μM) was prepared using 2 mL of the egg yolk extract, and the fluorescence spectrum was measured under the same experimental conditions.

Detection of cholesterol in goat blood

Following the collection of goat blood, a 10 μL aliquot was initially diluted ten-fold with buffer solution. From this stock, 200 μL was further diluted with 1790 μL of buffer. Subsequently, 10 μL of **ATBz** solution was added to the mixture, and the fluorescence spectra were recorded both in the absence and presence of cholesterol.

Paper strip-based detection of cholesterol

A simple and low-cost paper strip sensor for cholesterol detection was fabricated using **ATBz**. Small pieces of Whatman filter paper were cut and coated with **ATBz** solution. After drying, the strips were placed in a UV chamber, where no fluorescence was initially visible. When a drop of cholesterol solution was applied to the sensing area, a distinct green fluorescence appeared, confirming the presence of cholesterol.

Results and discussion

Structural characterization of ATBz

All the synthesized compounds were initially characterized using liquid chromatography-mass spectrometry (LC-MS). Compound **2** exhibited an $[M + H]^+$ peak at 270.20 Da (calculated for $C_{20}H_{15}N$ $[M + H]^+$, m/z = 270.12), **4** showed an $[M\text{-}N_2]$ peak at 104.70 Da (calculated for $C_7H_7N_3$ $[M\text{-}N_2]$, m/z = 105.06), and the final compound **ATBz** showed an $[M + H]^+$ peak at 536.50 Da (calculated for $C_{34}H_{29}N_7$ $[M + H]^+$, m/z = 536.25) (Fig. S1–S3). The ^{1}H and ^{13}C NMR spectra of the synthesized molecules were recorded in $CDCl_3$ at 298 K (Fig. 1a and Fig. S7–S12). For compound **2**, the protons corresponding to the alkyne group appeared as a triplet at 2.29 ppm (Fig. S6, type a), which disappears in the spectrum of the final product **ATBz** (Fig. 1a) after the click reaction. In the case of compound **4**, five aromatic protons appeared as a multiplet at 7.37 ppm (Fig. S9, type b), which are shielded to 7.29 ppm (types e–g) in **ATBz** due to the absence of the azide group. Additionally, the two $-CH_2-$ protons (Fig. S9, type a) appeared as a singlet at 4.37 ppm, which is deshielded to 5.41 ppm (type b) in **ATBz** attributed to the influence of the neighbouring electronegative nitrogen atom of the triazole ring. A sharp singlet at 7.32 ppm (type i) corresponding to the triazole ring proton confirms the successful formation of the final product. Further analysis was performed using Fourier Transform Infrared (FT-IR) spectroscopy (Fig. 1b and Fig. S4–S6). The dialkyne compound **2** exhibited a characteristic $-C\equiv C-H$ stretching vibration at 3286 cm^{-1}, while the diazide compound **4** displayed a strong $-N_3$ stretching band at 2090 cm^{-1}. In the FT-IR spectrum of the final product **ATBz**, disappearance of the alkyne and azide stretching bands along with the appearance of a new peak at 2922 cm^{-1}, corresponding to the triazole ring, confirms the successful completion of CuAAC reaction. The PXRD analysis of **ATBz** displays distinct and intense diffraction peaks, indicating that the assemblies possess a crystalline structure (Fig. S13).

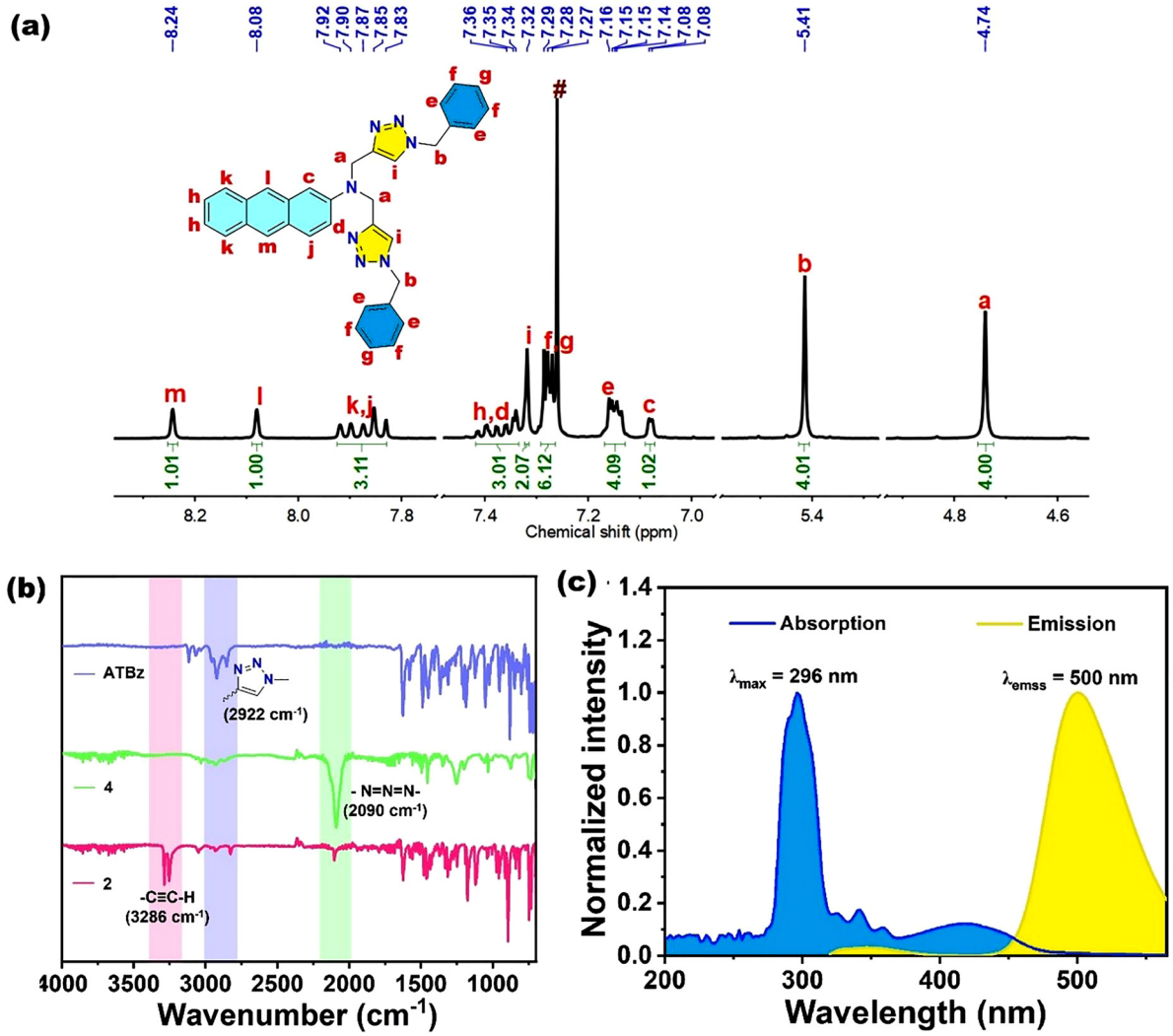

Fig. 1 (a) ^{1}H-NMR spectrum of **ATBz** at 400 MHz in $CDCl_3$ at 298 K, with (#) denoting the residual proton signal of $CDCl_3$, (b) FT-IR spectrum of **ATBz**, (c) Normalised absorption and emission spectra of **ATBz** (20 μM) in water (1% DMSO) upon excitation at 296 nm.

Photophysical studies of ATBz

Following the complete structural characterization of **ATBz**, its photophysical properties were investigated in various solvents (Fig. 1c and Fig. S14–S17). The UV-vis absorption and emission spectra of **ATBz** were recorded in different solvents such as toluene, dichloromethane (DCM), acetonitrile (ACN), and dimethyl sulfoxide (DMSO) at 25 °C. In toluene, the absorption spectrum of **ATBz** displays a sharp band at 296 nm, along with additional moderate-intensity bands at 324 nm, 340 nm, and 356 nm, accompanied by a tailing band around 412 nm. These absorption bands are attributed to the π–π* transitions of the aromatic rings of the anthracene moiety. Upon increasing solvent polarity from nonpolar toluene to polar solvents such as DCM, ACN, and DMSO, a slight red shift (2–6 nm) in the absorption maxima was observed (Fig. S14). The fluorescence spectrum in toluene shows an emission maximum at 469 nm, which progressively red-shifts to 479–500 nm with increasing solvent polarity (Fig. S15). The quantum yield of **ATBz** was determined in different solvent systems (Table S2). Compound **ATBz** exhibits a higher quantum yield in the polar solvent DMSO (0.66) and moderate quantum yields of 0.59, 0.57, and 0.54 in dichloromethane, methanol, and acetonitrile, respectively. The enhanced fluorescence efficiency in polar solvents can be attributed to the stabilization of the excited state, which provides a more favourable environment for radiative decay. In contrast, lower quantum yields were observed in toluene (0.47) and tetrahydrofuran (0.48), indicating that less polar solvents facilitate non-radiative pathways, thereby reducing emission efficiency.

We have further investigated the photophysical response of **ATBz** by gradually increasing the water fraction (f_w) in DMSO up to 99% (Fig. S16). **ATBz** is intrinsically emissive in DMSO. Upon increasing the water fraction up to 40%, controlled aggregation occurs, which restricts intramolecular motions and leads to enhanced emission. However, above ~50% water the solubility of **ATBz** drops sharply, causing the formation of large, disordered aggregates. These aggregates favour non-radiative decay

pathways, resulting in the observed fluorescence quenching. Thus, the quenching above 50% arises from poor solubility and excessive, disordered aggregation. Additionally, the quantum yield values in the water/DMSO mixtures (Table S3) indicate that from 0 to 40% water fraction, there is a gradual increase, reaching a maximum of 0.69 at 40%. However, beyond 40% water, the quantum yield decreases markedly, dropping to 0.25 in 80% water. The viscosity-dependent fluorescence behaviour of **ATBz** was examined using glycerol/DMSO mixtures (Fig. S17). The fluorescence intensity gradually rises as the glycerol content increases from 0% to 30%, suggesting that the moderately viscous environment restricts the intramolecular motion and decreases non-radiative relaxation, thereby strengthening the emission. In contrast, when the glycerol fraction exceeds 40%, a noticeable reduction in fluorescence is observed, likely due to the lower solubility of **ATBz** in highly viscous media. Consistent with this trend, the measured quantum yield values in glycerol/DMSO mixtures show a slight increase from 0.64 in pure DMSO to 0.67 in 20% glycerol; however, beyond this composition, the quantum yield progressively declines and sharply drops to 0.21 in 80% glycerol.

Detection of cholesterol using ATBz

The remarkable photophysical sensitivity of **ATBz** to its solvent microenvironment prompted us to explore its potential for sensing applications in aqueous media. A range of biologically relevant molecules and ions including cholesterol, cysteine, glutamic acid, histidine, phenylalanine, serine, tryptophan, valine, ascorbic acid, creatinine, dopamine, glucose, sucrose, urea, uric acid, and metal ions such as K^+, Na^+, Mg^{2+}, and Ca^{2+} were examined using fluorescence spectroscopy. Upon addition of various analytes (50 μM) to a solution of **ATBz** (10 μM) in water, a notable fluorescence enhancement was observed only in the presence of cholesterol. In contrast, the other analytes did not induce any significant change in the emission intensity, indicating the selectivity towards cholesterol (Fig. 2a and b). To further validate the interaction between **ATBz** and cholesterol, the fluorescence titration experiment was conducted in water containing 0.5% DMSO. Upon incremental addition of cholesterol (0–50 μM) to the **ATBz** solution, a pronounced enhancement in fluorescence intensity was observed, accompanied by a blue shift in the emission maximum from 498 nm to 486 nm ($\Delta\lambda$ = 12 nm) (Fig. 2c). The addition of cholesterol to the **ATBz**

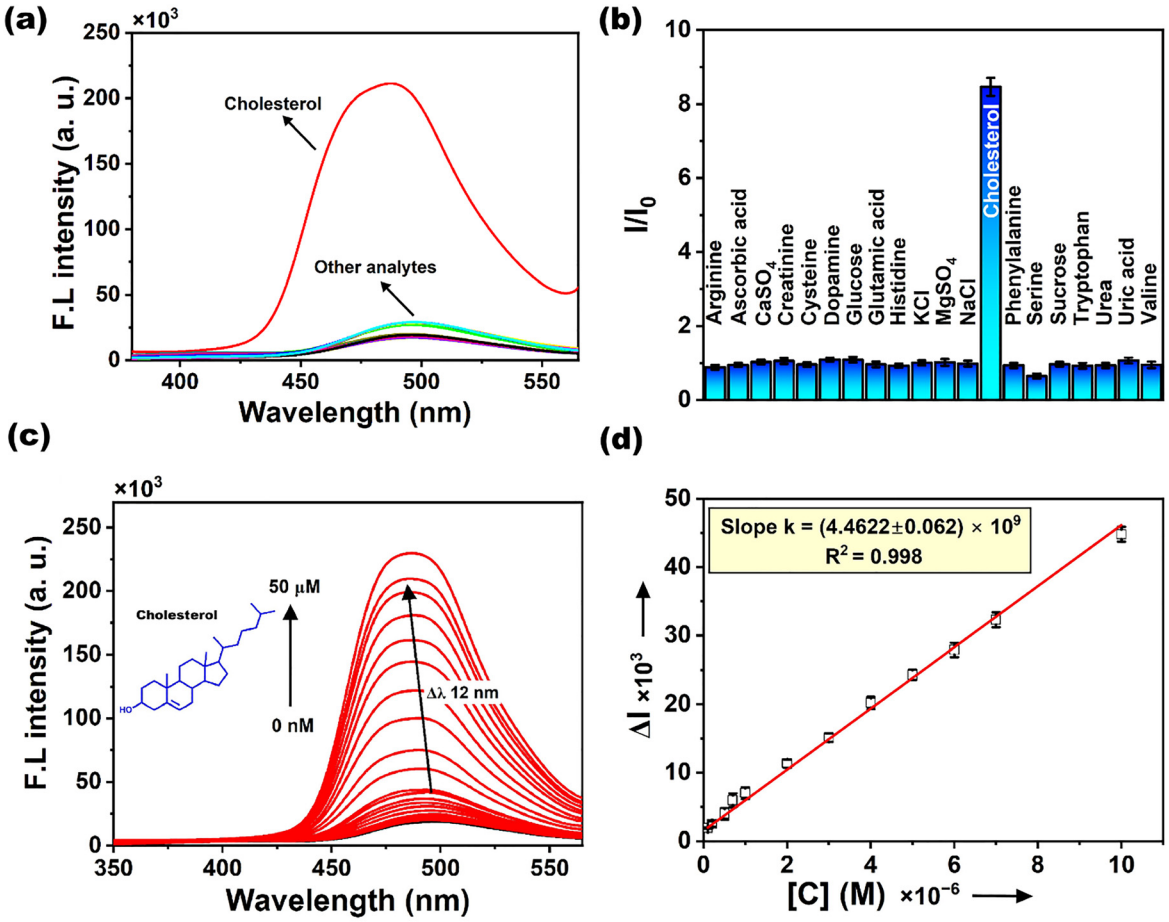

Fig. 2 (a) The selectivity of cholesterol with respect to the various analytes (50 μM) in water (0.5% DMSO) recorded at 25 °C when excited at 296 nm, (b) the bar diagram showing the selectivity for cholesterol in the presence of other analytes, (c) changes in the fluorescence profile of **ATBz** upon titration with various concentrations of cholesterol (0 μM to 50 μM) in water (0.5% DMSO) when excited at 296 nm, and (d) the fluorescence intensity *vs.* concentration of cholesterol plot.

solution resulted in a blue shift of the absorption band from 418 nm to 412 nm ($\Delta\lambda$ = 6 nm), accompanied by a noticeable flattening of the broad tail in the visible region (Fig. S18). This behaviour indicates the formation of more compact and well-organized nano-aggregates. Quantum yield measurements further confirmed this enhancement, increasing from 0.12 for **ATBz** to 0.76 after the addition of 50 μM cholesterol to the 10 μM sensor solution.

The binding constant (K_a) between **ATBz** and cholesterol was determined using the Benesi–Hildebrand method and calculated to be (1.29 ± 0.24) × 10^5 M^{-1}, indicating a strong interaction (Fig. S19). The limit of detection (LOD) for cholesterol, calculated using the $3\sigma/K$ method, was found to be 100 nM (± 1.4 nM) (Fig. 2d). Interestingly, upon interaction with cholesterol, **ATBz** exhibited a bright green emission accompanied by enhanced fluorescence (Fig. 3a). Furthermore, a gradual increase in cholesterol concentration from 0 to 1 mM led to a corresponding rise in the green emission intensity (Fig. S20). To evaluate potential interference, various biomolecules such as cysteine, glutamic acid, histidine, phenylalanine, serine, tryptophan, valine, ascorbic acid, creatinine, dopamine, glucose, sucrose, urea, and uric acid and metal ions including K^+, Na^+, Mg^{2+}, and Ca^{2+} were tested by adding them in the range of 5 mM to the **ATBz**–cholesterol system. However, none of these analytes caused any significant change in the fluorescence emission, indicating high selectivity of **ATBz** for cholesterol (Fig. 3b). The pH stability of **ATBz**, both in the absence and presence of cholesterol, was evaluated using a series of buffer solutions (Fig. S21). The sensor exhibited good stability across the tested pH range, although a moderate decrease in fluorescence intensity was observed under strongly acidic conditions. Notably, the **ATBz**–cholesterol complex demonstrated excellent stability within the physiological pH range.

Mechanistic study of cholesterol detection using ATBz

Time-correlated single photon counting (TCSPC) measurements of **ATBz** were performed in water containing 0.5% DMSO. **ATBz** alone exhibited a fluorescence lifetime of 6.03 ± 0.06 ns. Upon the addition of cholesterol (10–50 μM), the lifetime increased significantly, ranging from 7.88 ± 0.23 ns to 19.19 ± 0.08 ns (Fig. 3c). The observed increase in fluorescence lifetime corroborates the enhanced emission intensity of **ATBz** assemblies upon interaction with cholesterol. Dynamic light scattering (DLS) analysis was performed for the **ATBz**–cholesterol solution, and upon cholesterol addition, the particle size was observed to be 239 nm (Fig. S22). Furthermore, the **ATBz**–cholesterol solution

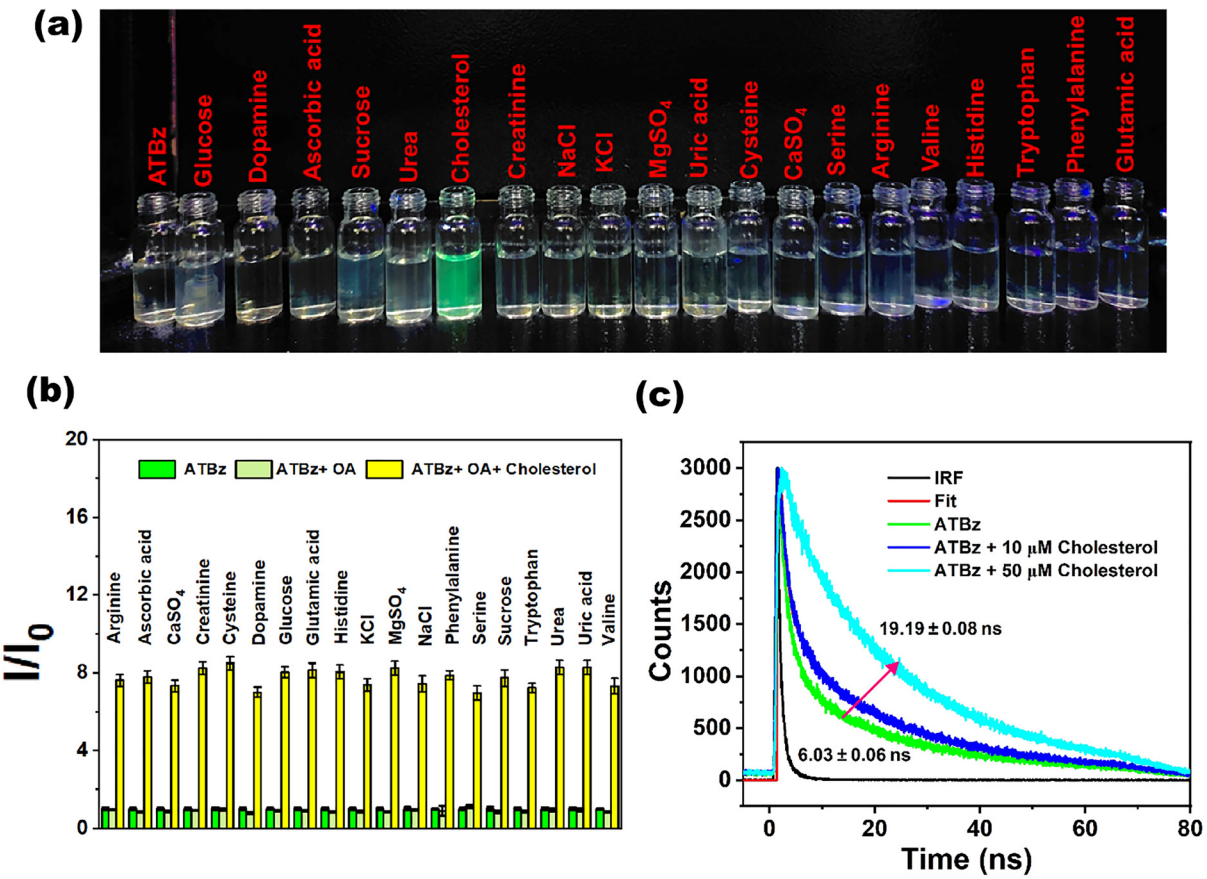

Fig. 3 (a) Photograph of **ATBz** with various analytes (100 μM) including cholesterol upon illumination under a UV lamp, (b) bar diagram representing competition in the presence of various analytes (OA = other analytes), and (c) the time-resolved fluorescence spectra of **ATBz** with 10 and 50 μM cholesterol concentration.

exhibited a distinct Tyndall effect (Fig. S23), preliminarily confirming the formation of nanoscale aggregates.

The formation of aggregates was further confirmed by field emission scanning electron microscopy (FESEM) analysis of **ATBz** before and after the addition of cholesterol (Fig. S24). In the absence of cholesterol, **ATBz** exhibits an irregular surface morphology (Fig. S24(a)). However, upon cholesterol addition, distinct and compact nano-aggregates are observed (Fig. S24(b)), with an average particle size of approximately ~237 nm, clearly demonstrating cholesterol-induced self-assembly. In addition, ^{1}H NMR spectra of **ATBz** were recorded with and without cholesterol addition (Fig. S25). The aromatic proton signals show a slight upfield shift, suggesting π–π stacking interactions arising from closer packing within the aggregates. Similarly, the aliphatic proton signals at 4.72 and 5.42 ppm exhibit upfield shifts and noticeable peak broadening, indicating restricted molecular motion and the formation of larger aggregated structures. Furthermore, upon cholesterol addition, the PXRD pattern reveals sharper and more intense diffraction peaks, demonstrating enhanced crystallinity (Fig. S26). This suggests that cholesterol promotes stronger molecular interactions with **ATBz**, leading to the development of more compact and highly ordered assemblies. Molecular docking studies were conducted to gain insight into the interaction between **ATBz** and cholesterol (Fig. S27). The aromatic components, including the benzyl substituents, triazole ring, and anthracene unit, participate in π–π stacking interactions, which likely arise from the closer molecular packing within the aggregates. Cholesterol functions as a structure-directing hydrophobic additive: it excludes polar protic solvent molecules, creates a locally hydrophobic microenvironment, and promotes the formation of more planar and rigid nano-assemblies. These ordered assemblies suppress non-radiative relaxation pathways and prevent uncontrolled aggregation that would otherwise lead to fluorescence quenching. Consequently, **ATBz** forms highly emissive aggregates only in the presence of cholesterol, resulting in significant fluorescence enhancement even at high water fractions.

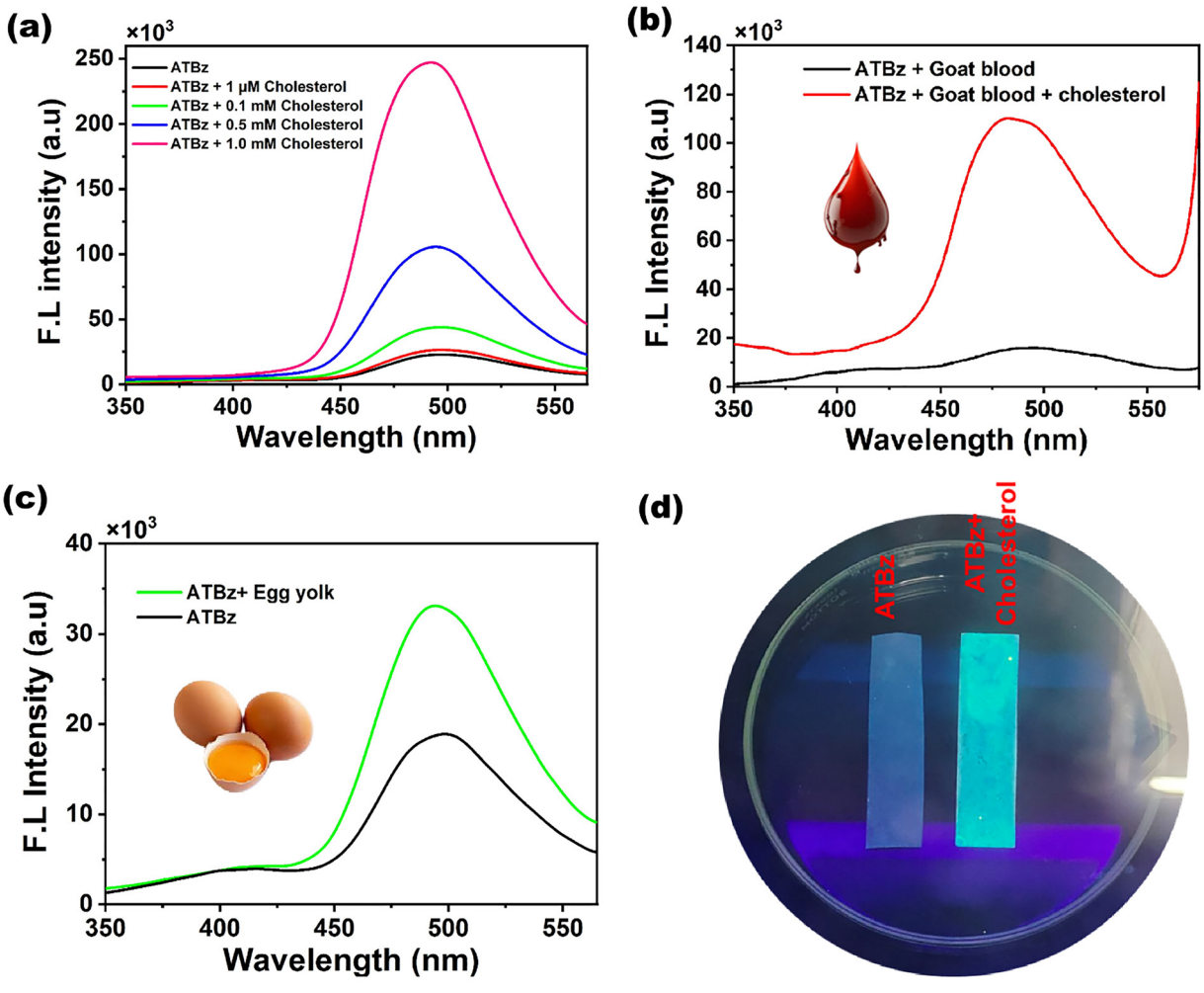

Fig. 4 Detection of cholesterol in (a) human serum, (b) goat blood and (c) egg yolk samples when excited at 296 nm. (d) Photograph of detection of cholesterol using an **ATBz** coated paper-strip under a UV lamp.

Table 1 Cholesterol recovery results in human serum samples

Sample	Added	Found (mean ± SEM)	Recovery (%)
Human serum	1 μM	1.08 ± 0.09 μM	108
	100 μM	103 ± 0.5 μM	103
	0.5 mM	0.49 ± 0.01 mM	98
	1 mM	0.97 ± 0.04 mM	97

Quantification of cholesterol in human serum

To validate the practical utility of this sensor, cholesterol sensing experiments were performed in human serum samples (Fig. 4a). The human serum samples were spiked with different known concentrations of cholesterol ranging from 1 μM to 1 mM. The obtained results, as summarized in Table 1, indicate that the experimentally measured cholesterol concentrations were in good agreement with the initially spiked values. The calculated recovery values, falling within the range of 97% to 108%, clearly demonstrate both the accuracy of detection and the robustness of the method in complex biological matrices such as serum.

Detection of cholesterol in goat blood, egg yolk, and paper strip

Cholesterol sensing was demonstrated in real goat blood, where the presence of cholesterol led to a marked increase in the fluorescence intensity of **ATBz** (Fig. 4b). Since egg yolk is naturally rich in cholesterol, the introduction of **ATBz** into egg yolk solutions also produced a noticeable enhancement in fluorescence intensity (Fig. 4c). Furthermore, cholesterol detection was also demonstrated using a paper-based strip. In this approach, **ATBz** solution was drop-cast onto the Whatman filter paper, which initially showed no fluorescence under UV light (Fig. 4d). Remarkably, upon treatment with cholesterol, the strip displayed enhanced fluorescence with a distinct green emission. These findings highlight the potential of **ATBz** as a promising probe for cholesterol detection in real-world and environmental samples.

Conclusions

In conclusion, we successfully designed and synthesized an anthracene–triazole-based molecular probe (**ATBz**) *via* copper-catalyzed azide–alkyne click reaction (CuAAC), employing anthracene alkyne and benzyl azide as precursors. The synthetic approach is straightforward and affords the product in good yield. The **ATBz** molecule exhibits selective interaction with cholesterol, leading to a significant fluorescence enhancement accompanied by green emission. This response was further validated using the Benesi–Hildebrand method and a nanomolar LOD, while competitive experiments confirmed the sensor's high selectivity. An increase in fluorescence lifetime supported the observed enhancement in the emission intensity of **ATBz** assemblies upon cholesterol binding. DLS measurements indicated a growth in the particle size in the presence of cholesterol and the **ATBz**–cholesterol solution displayed a clear Tyndall effect. FESEM, PXRD and ^{1}H NMR analyses further confirm the formation of cholesterol driven nanoscale aggregates. The practical applicability of **ATBz** was assessed through real-sample analysis, where cholesterol-spiked human serum exhibited recovery rates of 97–108%. Furthermore, cholesterol detection was demonstrated in goat blood and egg yolk samples and on paper strips, highlighting **ATBz** as a simple, rapid, enzyme- and metal-free fluorescent platform for real time monitoring of cholesterol in real-world and practical settings.

Author contributions

M. P. conceptualized the study on selective fluorescence detection of cholesterol using an anthracene–triazole probe: a turn-on, enzyme- and metal-free approach. M. P. and R. K. M. jointly developed the molecular design and synthetic strategies. R. K. M. carried out the synthesis, characterization, fluorescence measurements, and TCSPC studies. Data analysis was performed collaboratively by R. K. M. and M. P. The manuscript was written by R. K. M and M. P.

Conflicts of interest

There are no conflicts to declare.

Data availability

The data will be made available upon request to the authors.

Supplementary information is available (SI). See DOI: https://doi.org/10.1039/d5tc03858h.

Acknowledgements

We sincerely acknowledge the Central Instrumentation Facility (CIF) at IIT Palakkad for providing instrumentation support, the Central Instrumentation Centre (CIC) of Bharathiar University for access to the NMR facility, the Exploratory Research Grant IIT Palakkad, and University Grants Commission (UGC) for financial assistance.

References

1 F. R. Maxfield and G. van Meer, Cholesterol, the central lipid of mammalian cells, *Curr. Opin. Cell Biol.*, 2010, **22**, 422–429.
2 I. Tabas, Cholesterol in health and disease, *J. Clin. Invest.*, 2002, **110**, 583–590.
3 W. Xiao, Z. Yang, J. Liu, Z. C. Chen and H. Li, Sensitive cholesterol determination by β-cyclodextrin recognition based on fluorescence enhancement of gold nanoclusters, *Microchem. J.*, 2022, **175**, 107125.
4 X. Wang and L. Hu, Review-Enzymatic Strips for Detection of Serum Total Cholesterol with Point-of-Care Testing (POCT) Devices: Current Status and Future Prospect, *J. Electrochem. Soc.*, 2020, **167**, 037535.

5 A. Zampelas and E. Magriplis, New Insights into Cholesterol Functions: A Friend or an Enemy?, *Nutrients*, 2019, **11**, 1645.
6 P. K. Morgan, L. Fang, G. I. Lancaster and A. J. Murphy, Hematopoiesis is regulated by cholesterol efflux pathways and lipid rafts: Connections with cardiovascular diseases, *J. Lipid Res.*, 2020, **61**, 667–675.
7 H. Y. Chen, P. L. Xin, H. Bin Xu, J. Lv, R. C. Qian and D. W. Li, Self-Assembled Plasmonic Nanojunctions Mediated by Host-Guest Interaction for Ultrasensitive Dual-Mode Detection of Cholesterol, *ACS Sens.*, 2023, **8**, 388–396.
8 F. M. Feringa and R. van der Kant, Cholesterol and Alzheimer's Disease; From Risk Genes to Pathological Effects, *Front. Aging Neurosci.*, 2021, **13**, 1–17.
9 Y. Zhang, E. Vittinghoff, M. J. Pletcher, N. B. Allen, A. Zeki Al Hazzouri, K. Yaffe, P. P. Balte, A. Alonso, A. B. Newman, D. G. Ives, J. S. Rana, D. Lloyd-Jones, R. S. Vasan, K. Bibbins-Domingo, H. C. Gooding, S. D. de Ferranti, E. C. Oelsner and A. E. Moran, Associations of Blood Pressure and Cholesterol Levels During Young Adulthood with Later Cardiovascular Events, *J. Am. Coll. Cardiol.*, 2019, **74**, 330–341.
10 S. R. Hu, C. R. Yang, Y. F. Huang, C. C. Huang, Y. L. Chen and H. T. Chang, Ratiometric Fluorescence Probe of Vesicle-like Carbon Dots and Gold Clusters for Quantitation of Cholesterol, *Chemosensors*, 2022, **10**, 1–13.
11 N. R. Nirala, S. Abraham, V. Kumar, A. Bansal, A. Srivastava and P. S. Saxena, Colorimetric detection of cholesterol based on highly efficient peroxidase mimetic activity of graphene quantum dots, *Sens. Actuators, B*, 2015, **218**, 42–50.
12 O. López-Fernández, R. Domínguez, E. M. Santos, M. Pateiro, P. E. S. Munekata, P. C. B. Campagnol and J. M. Lorenzo, Comparison Between HPLC-PAD and GC-MS Methods for the Quantification of Cholesterol in Meat, *Food Anal. Methods*, 2022, **15**, 1118–1131.
13 (*a*) P. Linsel-Nitschke and A. R. Tall, HDL as a target in the treatment of atherosclerotic cardiovascular disease, *Nat. Rev. Drug Discovery*, 2005, **4**, 193–205; (*b*) M. M. Rahman, X. B. Li, J. Kim, B. O. Lim, A. J. S. Ahammad and J. J. Lee, A cholesterol biosensor based on a bi-enzyme immobilized on conducting poly(thionine) film, *Sens. Actuators, B*, 2014, **202**, 536–542.
14 Y. Huang, J. Tan, L. Cui, Z. Zhou, S. Zhou, Z. Zhang, R. Zheng, Y. Xue, M. Zhang, S. Li, N. Zhu, J. Liang, G. Li, L. Zhong and Y. Zhao, Graphene and Au NPs co-mediated enzymatic silver deposition for the ultrasensitive electrochemical detection of cholesterol, *Biosens. Bioelectron.*, 2018, **102**, 560–567.
15 L. Yu, Y. Shen, L. Chen, Q. Zhang, X. Hu and Q. Xu, Molecularly imprinted ultrasensitive cholesterol photoelectrochemical sensor based on perfluorinated organics functionalization and hollow carbon spheres anchored organic-inorganic perovskite, *Biosens. Bioelectron.*, 2023, **237**, 115496.
16 (*a*) N. Zhang, Y. Liu, L. Tong, K. Xu, L. Zhuo and B. Tang, A novel assembly of Au NPs-β-CDs-FL for the fluorescent probing of cholesterol and its application in blood serum, *Analyst*, 2008, **133**, 1176–1181; (*b*) D. M. Amundson and M. Zhou, Fluorometric method for the enzymatic determination of cholesterol, *J. Biochem. Biophys. Methods*, 1999, **38**, 43–52.
17 U. Hanefeld, L. Cao and E. Magner, Enzyme immobilisation: Fundamentals and application, *Chem. Soc. Rev.*, 2013, **42**, 6211–6212.
18 (*a*) Z. Qing, A. Bai, S. Xing, Z. Zou, X. He, K. Wang and R. Yang, Progress in biosensor based on DNA-templated copper nanoparticles, *Biosens. Bioelectron.*, 2019, **137**, 96–109; (*b*) C. Song, W. Hong, X. Zhang and Y. Lu, Label-free and sensitive detection of Ochratoxin A based on dsDNA-templated copper nanoparticles and exonuclease-catalyzed target recycling amplification, *Analyst*, 2018, **143**, 1829–1834; (*c*) Z. Qing, J. Xu, J. Hu, J. Zheng, L. He, Z. Zou, S. Yang, W. Tan and R. Yang, In Situ Amplification-Based Imaging of RNA in Living Cells, *Angew. Chem., Int. Ed.*, 2019, **58**, 11574–11585.
19 H. Abed, R. Sabouni and M. Ghommem, MOF-based spectrophotometric sensors for cholesterol detection: current trends and challenges, *RSC Adv.*, 2024, **14**, 39472–39497.
20 X. Ye, Y. Jiang, X. Mu, Y. Sun, P. Ma, P. Ren and D. Song, Ultrabright silicon nanoparticle fluorescence probe for sensitive detection of cholesterol in human serum, *Anal. Bioanal. Chem.*, 2022, **414**, 3827–3836.
21 N. Sultana, S. V. Andagonde, R. Chakraborty, A. Bala and N. Sen Sarma, A non-enzymatic dual sensing approach for the detection of cholesterol in real samples using silk fiber functionalized phosphorene quantum dots, *Nanoscale*, 2024, **17**, 3042–3052.
22 J. Dolai, H. Ali and N. R. Jana, Selective capturing and fluorescence ''turn on'' detection of dibutyl phthalate using a molecular imprinted nanocomposite, *New J. Chem.*, 2021, **45**, 19088–19096.
23 A. Kaur, M. Kumar and V. Bhalla, Enzyme-/metal-free quinoxaline assemblies: direct light-up detection of cholesterol in human serum, *Chem. Commun.*, 2023, **59**, 1501–1504.
24 Y. Wu, X. Fang, L. Lin, H. Guo and F. Yang, A double-ionic macrocycle based on cyanostilbene: First organic fluorescence sensor based small molecular system for detecting cholesterol, *Bioorg. Chem.*, 2025, **160**, 108483.